A MID-FIDELITY AEROELASTIC COUPLING FRAMEWORK FOR ANALYZING FLUTTER DYNAMICS IN ROTORCRAFT APPLICATIONS

Moritz Linder
Research Associate

Muhammed Kürşat Yurt
Research Associate

İlkay Yavrucuk
Professor

Institute for Rotorcraft and Vertical Flight
Technical University of Munich
Munich, Germany

ABSTRACT

An aeroelastic coupling framework is presented, based on a time-resolved 3D surface-based coupling between a mid-fidelity aerodynamic solver (UPM) and a modal structural solver (HTModal). The aim is to improve the aeroelastic prediction quality with regard to dynamic phenomena, stability, and flutter in rotorcraft applications by enabling these phenomena to be accurately predicted in simulations, taking into account interaction effects. In this paper, the presented coupling framework is validated with different test cases. For this purpose, fixed-wing benchmark test cases presented in the literature (Goland, Pazy) are used to verify the prediction accuracy with regard to flutter speeds, as well as hover test data from the whirl tower test bench of the Institute for Rotorcraft and Vertical Flight at the Technical University of Munich to demonstrate the accuracy of the simulation, specifically in rotorcraft applications. The simulation results show good agreement with the test results, both in the static deformation analysis and in the dynamic stability and flutter analysis. Thus, the presented surface-based mid-fidelity coupling approach offers a promising approach for the analysis of arbitrary structures and shapes in rotorcraft applications.

NOTATION

*

Symbols

c Aerodynamic chord

C_p Pressure coefficient

$\boldsymbol{D}$ Damping-matrix

$\boldsymbol{D}_{mod}$ Modal damping-matrix

D_n Damping constant of mode n

f Frequency

$\boldsymbol{F}$ Load vector

$\boldsymbol{F}_{mod}$ Modal load vector

I_j Moment of inertia about axis j

$\boldsymbol{K}$ Stiffness-matrix

$\boldsymbol{K}_{mod}$ Modal stiffness-matrix

$\boldsymbol{M}$ Mass-matrix

$\boldsymbol{M}_{mod}$ Modal mass-matrix

N Number of degrees of freedom

N_b Number of blades

R Rotor radius

U_∞ Free-stream velocity

$\boldsymbol{x}$ Displacement vector

$\boldsymbol{\zeta}$ Damping vector

ζ_n Modal damping coefficient of mode n

$\boldsymbol{\xi}$ Modal displacement vector

$\boldsymbol{\Phi_n}$ Eigenvector of mode n

ω Natural eigenfrequency

$\boldsymbol{\omega}$ Frequency vector

ω_n Eigenfrequency of mode n

Ω Rotational speed

ρ Air density

*

Acronyms

AoA Angle of attack

AR Aspect ratio

CFD Computational fluid dynamics

CG Center of gravity

CSD Computational structural dynamics

DIC Digital Image Correlation

DLR German Aerospace Center

DoF Degree of freedom

EA Elastic axis

ERA Eigensystem Realization Algorithm

FE Finite element

MERIT Munich Experimental Rotor Investigation Testbed

OMA Operational Modal Analysis

UPM Unsteady Panel Method

VPM Vortex particle method

VTOL Vertical take-off and landing vehicle

INTRODUCTION

The design of new helicopters and innovative rotorcraft and VTOL (vertical take-off and landing) concepts pose a major challenge due to the high complexity of the vehicles, both in terms of aerodynamic interactions and the resulting interference, and in terms of dynamics and stability behaviour. In particular, novel concepts with an increasing number of propellers and wing structures with increased structural elasticity place high demands on the prediction tools used. This is why the development of these numerical aeroelastic tools remains a central component of research and development, despite significant progress in recent years (Refs. 1–4). Due to the highly complex aeroelastic interaction phenomena, which often occur only in a very limited range of the flight envelope under special conditions, potential instabilities are often only discovered in late development phases, which results in high costs and prolongs development time (Ref. 5). This applies not only to new VTOL concepts, but also to classic helicopter configurations, as examples such as the S-76 (Ref. 6) or EH-101 (Ref. 7) show. This underscores the need for efficient and accurate numerical prediction tools in order to model and analyse the occurring phenomena as efficiently and early as possible in the development process, thereby enabling potential instabilities to be detected and adjustments to be made.

When analysing stability behaviour, particularly in highly elastic and flexible structures, it is of high importance that both the aerodynamics and the structural behaviour are modelled correctly in order to be able to map the mutual influence and analyse the overall aeroelastic behaviour. The structural response to aerodynamic loads has to be modelled correctly in order to predict the occurring deformations and potentially excited vibrations, which in turn influence the aerodynamic flow and load conditions again. Numerous studies using high-fidelity computational fluid dynamics (CFD) have shown that these viscous simulation approaches can accurately reproduce both low-frequency phenomena, relevant for example for investigating phenomena like tail shake, and high-frequency flow phenomena caused by blade passage interactions (Refs. 8–10). Couplings of these high-fidelity CFD methods with computational structural dynamics (CSD) methods have also been successfully implemented and investigated, enabling the analysis of a wide variety of aeroelastic phenomena. For example, this approach has been successfully used to predict the flutter behaviour of a fin model (Ref. 11), as well as to investigate resonances, aerodynamic damping factors and loads in the case of the tail shake phenomenon (Ref. 12). The major disadvantage of these methods is the considerable time required to create the models and perform the simulations themselves, which limits their applicability, particularly in early development stages and optimisation processes.

In this area in particular, transient panel and vortex particle methods (VPM) show promising approaches due to their significantly reduced computing times, while still guaranteeing good accuracy and the possibility to model interactions (Refs. 13, 14). Aeroelastic couplings have also already been successfully implemented with this approach, such as the coupling of the vortex particle solver *DUST* with the multibody structural solver *MBDyn*. The structure is represented by 1D elements in this particular approach, while the aerodynamics can be modelled using either a vortex lattice or surface panels. This coupling framework has been used to successfully analyse benchmark test cases and conduct investigations on tilt rotors, demonstrating the applicability of such approaches for predicting interactions, vibrations and possible instabilities in early design phases (Ref. 15).

The mid-fidelity coupling framework presented in this paper is based on the tight surface-based coupling between a panel freewake aerodynamics solver and a modal structural solver presented in an earlier publication by the authors (Ref. 16). By using a surface-based coupling approach with panel modelling and a modal structural model, it is possible to model and analyse arbitrary shapes and structures without the need for complex transformations and mappings. The previous publication presented an initial implementation, which has already been successfully applied in a feasibility study on a complete helicopter simulation. This initial implementation is further developed and improved in this paper and validated using various test cases. For this purpose, different static and dynamic investigations are carried out. The first test case is the widely used Goland wing flutter test case. The second test case examined is the Pazy wing, which experiences large elastic deformations due to its low stiffness. For the last test case, hover test data from the institute's whirl tower rotor test bench, MERIT (Munich Experimental Rotor Investigation Testbed), is used to demonstrate the applicability of the framework in rotating systems.

SIMULATION FRAMEWORK

Freewake Solver

The developed coupling framework and the simulations performed in this work primarily use the Unsteady Panel Method (UPM), developed by the German Aerospace Centre (DLR) – Institute of Aerodynamics and Flow Technology (Refs. 17, 18). UPM is an unsteady three-dimensional panel-free wake code with a velocity-based indirect potential formulation. There are two different types of components (lifting and non-lifting components) that can be used to model the investigated configuration in UPM. For modelling lifting bodies, such as rotor blades or wings, sources and sinks are distributed on the surface of the body to represent the thickness effect, with an additional distribution of vortex elements on the camber surface, which models the lift (see Figure 1). Kutta panels are placed on the trailing edge of lifting bodies in tangential extension of the camber surface in order to model the shedded wake, consisting of vortex filaments, over the entire span. Non-lifting components are modelled exclusively with a source/sink distribution on the surface, which means that only the displacement effect on the flow is modelled, but not the generated lift and drag (Refs. 17, 19).

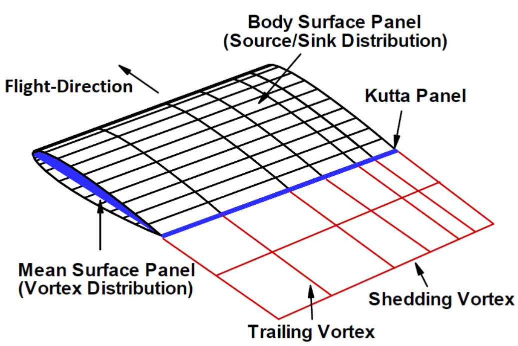

Figure 1: Schematic illustration of the modelling of lifting components in UPM (Ref. 13)

The wake of lifting components consists of quadrilateral vortex rings by default. The strength of the vortex rings, which are generated in each time step, corresponds to the strength of the Kutta panels and remains constant for each vortex ring over the simulation time. An explicit time step method is used for calculating the transient behaviour of the wake, which ensures that the wake is transported and deformed in accordance with the prevailing local flow conditions. In addition to the vortex panels, a vortex particle method is implemented, which offers the possibility of converting the vortex filaments into vortex particles in order to analyse particularly demanding interaction phenomena with large numbers of components (Refs. 20, 21).

For a direct comparison of different methods, the coupling presented in section Coupling Framework is also implemented using the VPM code DUST. DUST was developed at the Politecnico di Milano and has already been successfully coupled with the multi-body code MBDyn (Ref. 15). For a detailed description of the implementation of DUST, please refer to the work of Tugnoli et al. (Ref. 22). In this paper presented here, DUST is also coupled with the modal solver HTModal to enable a direct comparison of different modelling and coupling approaches.

Structural Solver

A computational structural dynamics (CSD) solver based on a modal approach is used for accurate modelling of the structure. This makes it possible to analyse the structural dynamics of arbitrarily complex shapes and structures in a computationally efficient manner by using the eigenmodes and eigenfrequencies of the structure. For very large models, the formulation in modal space gives the opportunity for the modal reduction approach to keep the computational effort low. The modal representation of the overall structure can be determined by modal analysis. The principle behind this is explained below.

The dynamic behaviour of a system with multiple DoFs N can be expressed by the following general equation of motion (Ref. 23):

$$\mathbf{M}\ddot{\mathbf{x}}(t) + \mathbf{D}\dot{\mathbf{x}}(t) + \mathbf{K}\mathbf{x}(t) = \mathbf{F}(t) \tag{1}$$

with:
- $\mathbf{M}$ Mass-matrix ($N \times N$)
- $\mathbf{D}$ Damping-matrix ($N \times N$)
- $\mathbf{K}$ Stiffness-matrix ($N \times N$)
- $\mathbf{x}$ Displacement vector
- $\mathbf{F}$ Load vector

If the displacements are assumed to be small, the structural behaviour can be assumed to be linear, which in turn allows the matrices to be linearised. Since determining the physical damping properties is not trivial and the exact values are therefore often unknown, an undamped structure is assumed for the transformation into modal space, and the damping is reintroduced later in the modal space. By neglecting the damping and using a harmonic approach, the following equation can be established for free vibration (Ref. 23):

$$\left(\mathbf{K} - \omega^2 \mathbf{M}\right) \boldsymbol{\Phi} = 0 \tag{2}$$

with:
- ω Natural eigenfrequency
- $\boldsymbol{\Phi}$ Eigenvector

Here, each eigenvalue ω_n (frequency) and eigenvector $\boldsymbol{\Phi}_n$ (mode shape) defines a natural mode representing one of the N degrees of freedom of the structure. The solutions of equation 2 are orthogonal and thus unique and cannot be converted into each other by linear superposition. If the eigenmodes are additionally normalised by mass, the modal mass M_n, modal stiffness K_n, and modal load F_n for each mode n can be obtained as follows:

$$M_n = \mathbf{\Phi}_n^T \mathbf{M} \mathbf{\Phi}_n = 1 \quad (3)$$

$$K_n = \mathbf{\Phi}_n^T \mathbf{K} \mathbf{\Phi}_n = \omega_n^2 \quad (4)$$

$$F_n = \mathbf{\Phi}_n^T \mathbf{F} \quad (5)$$

The damping value D_n of the corresponding eigenmode is defined in modal space according to equation 6. The modal damping value ζ_n is determined empirically and is usually in the range between 1 and 10% for aerospace structures (Ref. 24).

$$D_n = 2\omega_n \zeta_n \quad (6)$$

From the individual modal values, the corresponding matrices from equation 1 can be transformed into modal space according to equations 4–5, and together with the modal displacements $\boldsymbol{\xi}$, equation 1 can be formulated in modal space:

$$\mathbf{M}_{mod}\ddot{\boldsymbol{\xi}}(t) + \mathbf{D}_{mod}\dot{\boldsymbol{\xi}}(t) + \mathbf{K}_{mod}\boldsymbol{\xi}(t) = \mathbf{F}_{mod}(t) \quad (7)$$

$$\ddot{\boldsymbol{\xi}}(t) + 2\boldsymbol{\omega}\boldsymbol{\zeta}\dot{\boldsymbol{\xi}}(t) + \boldsymbol{\omega}^2\boldsymbol{\xi}(t) = \mathbf{F}_{mod}(t) \quad (8)$$

with:

$\mathbf{M}_{mod}$	Modal mass-matrix ($N \times N$)
$\mathbf{D}_{mod}$	Modal damping-matrix ($N \times N$)
$\mathbf{K}_{mod}$	Modal stiffness-matrix ($N \times N$)
$\mathbf{F}_{mod}$	Modal excitation
$\boldsymbol{\xi}$	Modal displacement vector
$\boldsymbol{\omega}$	Frequency vector
$\boldsymbol{\zeta}$	Damping vector

The modal solver used in this work is the structural solver *HTModal*, developed at the Institute for Rotorcraft and Vertical Flight, and was implemented specifically for time-resolved implicit aeroelastic coupling applications. An in-house development was chosen in order to have the option of easily supplementing the solver and integrating all necessary functionalities. HTModal can be used to solve both linear static and dynamic analysis problems. The dynamic calculations are based on the general equation of motion in modal space (see equation 8), using second-order time integration. Different time integration methods are implemented (e.g. Newmark-β method or Generalised-α method) with varying numerical damping. By limiting the frequency range relevant to the respective application, the computational effort can be reduced through modal reduction. Structural damping is applied depending on the respective eigenfrequency ω_n according to equation 6, whereby the individual modal damping coefficients ζ can be defined in different ways (e.g. uniform damping for all eigenmodes or a damping matrix specifying the modal damping for each mode).

The input files for HTModal are primarily based on the result files from NASTRAN's linear eigenvalue analysis (SOL103). The mass matrix, eigenvalues, and eigenvectors are required as necessary inputs from NASTRAN. In addition, the mesh of the structural model must be specified. Optionally, the structural and viscous damping matrices can be specified, if available, in order to calculate the corresponding modal damping coefficients. All specified matrices are transformed from physical to modal space using the eigenvectors and then used by the solver for the numerical calculation. The force vector can either be given manually as an input or, as in this coupling, passed from the aerodynamic solver via the coupling interface. After the structural calculation, the results (translatory and rotational displacements, velocities, and accelerations) are transformed back into physical space and stored in corresponding output files, and, if necessary, fed back to the coupling interface.

Coupling Framework

The coupling environment developed and improved in this work is a tight UPM-HTModal coupling framework utilising *preCICE*, an open-source coupling library for partitioned multi-physics simulations (Ref. 25). Figure 2 shows a schematic representation of the implemented aeroelastic coupling. The primary focus was on the application of UPM and HTModal in the framework, but due to the high modularity of the coupling library preCICE, the individual components of the coupling can be replaced relatively easily by other solvers. Therefore, in order to have a direct comparison between different methods, a DUST-HTModal coupling was also implemented. However, since the frameworks themselves are very similar, only the UPM-HTModal coupling will be discussed in the following, as this also forms the primary framework.

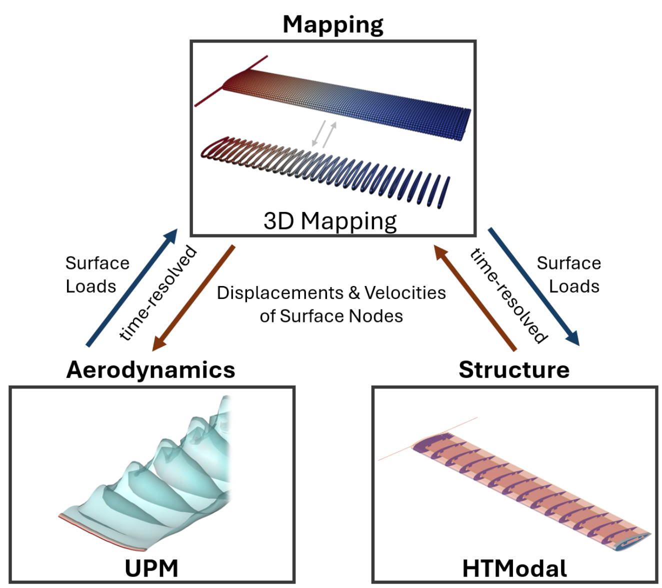

Figure 2: Schematic representation of the coupling framework

Tight coupling in the context of this work here refers to a time-resolved data exchange between UPM and HTModal. The surface data, i.e. the surface loads and the displacements and velocities of the surface nodes, are mapped directly in 3D between the respective meshes. This offers the possibility of using any aerodynamic shapes and structures directly in the coupling environment without transforming the data first. In addition, a wide variety of modelling approaches can be used for the structure, such as simple beam modelling or more complex 3D FE-models.

The preCICE coupling library is used to simplify the coupling process and ensure maximum modularity and adaptability. It offers various options in terms of coupling schemes and mapping algorithms. For the aeroelastic coupling implemented here, a serial implicit coupling scheme is used with optional and individual sub-cycling of the individual solvers. Figure 3 graphically illustrates the used coupling scheme. Before entering the coupling routine, there is the option of performing a stand-alone aerodynamic calculation over several time steps, the solution of which is then used to initialise the structural solver. This offers the possibility of fully developing the flow field and wake without the computationally intensive aeroelastic iteration loops. Alternatively, a so-called "fade-in" phase can be defined at the beginning of the coupling, in which the calculated aerodynamic loads are gradually increased to the nominal value. This can help to reduce the calculation time, especially for highly elastic structures, by significantly reducing overshoots at the beginning of the simulation caused by the sudden application of loads.

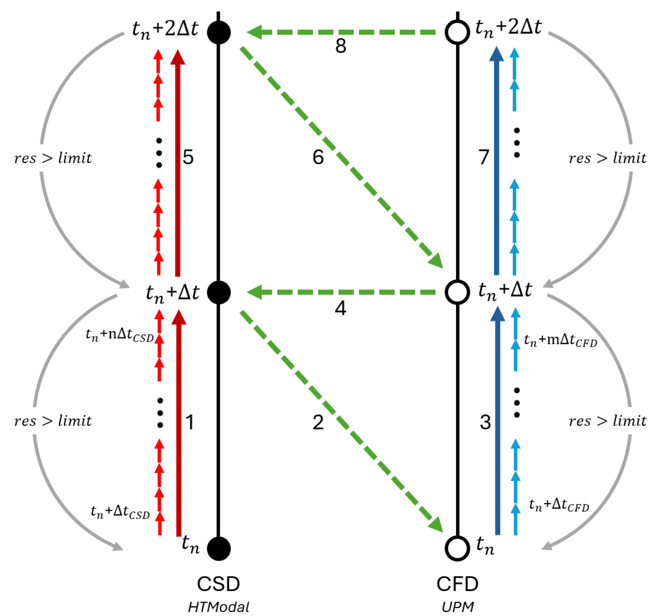

Figure 3: Serial implicit aeroelastic coupling scheme between CSD solver HTModal and CFD solver UPM with individual sub-cycling

The coupling time step at time t_n starts with the calculation of the structural response according to the current load state. To improve convergence and stability, the coupling time step Δt is subdivided into smaller time steps Δt_{CSD}. After calculating the equation of motion for the time step $(t_n \rightarrow t_n + \Delta t)$, the updated displacements and velocities are transferred to the aerodynamics solver, whereupon the time step $(t_n \rightarrow t_n + \Delta t)$ is calculated with the current deformation state. Here, too, a smaller time step Δt_{CFD} can be selected to improve numerical stability. After calculating the updated aerodynamic loads for the time step $(t_n \rightarrow t_n + \Delta t)$, these are fed back to the structural solver. Since an implicit method is used, convergence in the current time step is then checked using a specified criterion. If this is not satisfied, the time step $(t_n \rightarrow t_n + \Delta t)$ is recalculated with the updated deformation and load state. If the convergence criterion is satisfied, the next time step $(t_n + \Delta t \rightarrow t_n + 2\Delta t)$ is calculated, starting with the structural calculation. The size of the time step Δt should be selected so that all relevant frequencies can be resolved. For the sub-time steps, the investigations have shown that a default value of $1e-7s$ for Δt_{CSD} and a default value of $1/50f$ for Δt_{CFD} deliver good results, where f corresponds to the maximum frequency to be resolved.

For data mapping a simple nearest-neighbour approach is used in order to keep the mesh requirements and the computing time as low as possible. Figure 4 shows the mapping of the displacements from the HTModal mesh to the UPM mesh based on the example of the simple rectangular Pazy wing. To ensure correct mapping, additional model conversion routines were implemented to improve and simplify the mapping between different meshes, thereby preventing mapping errors, especially in cases where the meshes use different coordinate or unit systems.

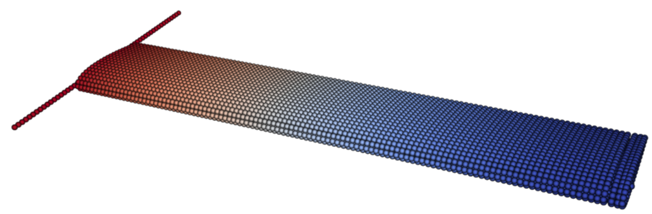

(a) Displacements on HTModal mesh

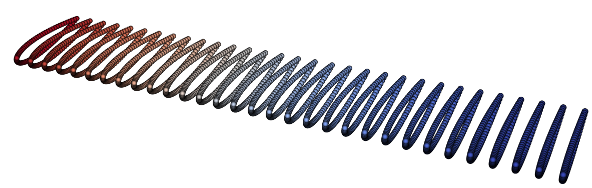

(b) Displacements on UPM mesh

Figure 4: Mapping of the wing displacements from HTModal mesh to UPM mesh

Two different meshes are used on the UPM side of the coupling. The first mesh consists of the collocation points of the individual panels and is used to transfer the aerodynamic loads to the structural mesh. The second mesh consists of the corner points of the panels and is used to apply the displacements and velocities transferred by the structural solver. This division into two different meshes also makes it possible to define different components in them. For example, in many cases, it makes sense to use the entire structure with all components included for the corner point mesh, while only selected components are included in the collocation point mesh. This allows parts that are not relevant for the aeroelastic analysis to be excluded. This can be used, for example, for the exclusion of non-lifting bodies from the collocation point mesh. Since in panel methods, the load calculations for non-lifting bodies are often less reliable than for lifting bodies, it can make sense to exclude them for load transfer. However, for the application of the deformation state, it still makes sense to apply it to the non-lifting bodies as well. This specific exclusion/inclusion of individual components is greatly simplified by having different meshes.

For the evaluation of the deformation data, the coordinate system definition with x in the span/radial direction, y from the trailing edge to the leading edge, and z in the thrust direction is always assumed in the following.

GOLAND WING

Setup and Models

As the first test case for validating the UPM-HTModal coupling framework, the wing flutter case by Goland (Ref. 26) is analysed, which is widely used in the literature as a test and validation case for aeroelastic codes. The Goland wing is a cantilevered wing with a rectangular planform and an aspect ratio (AR) of approximately 3.33, which means that three-dimensional aerodynamic effects have an influence on the aeroelastic behaviour. Figure 5 shows the fundamental layout of the wing with the position of the elastic axis (EA), the position of the centre of gravity axis (CG), and the free stream velocity U_∞, as well as the clamping. The wing properties and the basic flow condition are listed in Table 1 and are taken from (Ref. 26).

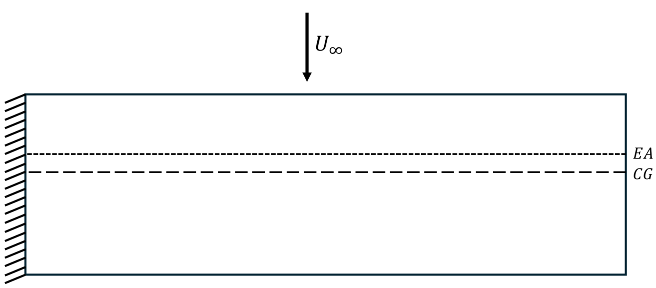

Figure 5: Goland cantilevered wing model layout

For modelling the structure, a combination of beam and shell elements was chosen, which are connected to each other via rigid body elements in the chord direction (see Fig. 6). The beam elements form the load-bearing structure, while the shell elements represent only the outer aerodynamic shape. Based on the values given in the literature, the stiffness and mass properties of the model were optimised in order to achieve the eigenfrequencies specified in the literature. The optimised structural parameters correspond well with the structural literature values, except for the inertia per unit span, which had to be reduced to $7.4 kgm$ in order to obtain a good match of the eigenfrequencies.

The comparison of the simulated eigenfrequencies with the literature values is listed in Table 2. The respective eigenmodes (1st and 2nd torsion and flap) are shown in Figure 7.

Table 1: Properties of the Goland wing and flow condition (Ref. 26)

Wing properties	
Half span	6096 mm
Chord (c)	1828.8 mm
Position EA	$0.33 * c$
Position CG	$0.43 * c$
Inertia per unit span	8.64 $kg\ m$
Mass per unit span	35.71 $kg\ m^{-1}$
Flap bending stiffness	$9.77 * 10^6\ N\ m^2$
Torsional stiffness	$0.99 * 10^6\ N\ m^2$
Flow condition	
Air density (ρ)	1.02 $kg\ m^{-3}$
AoA perturbation	0.05 deg

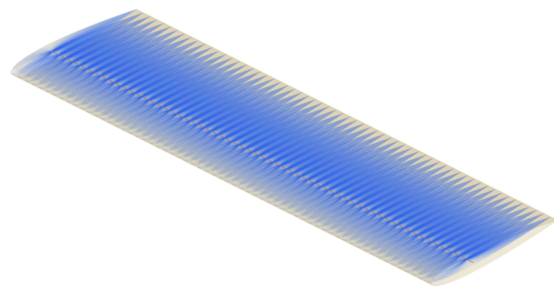

Figure 6: Representation of the structural Goland model

For the modelling of the aerodynamics, the NACA0012 profile was discretised with surface panels, with 30 panels in the spanwise direction and 40 panels in the chordwise direction, with a half-cosine refined distribution at the leading edge.

Table 2: Comparison of the eigenfrequencies for the fitted Goland FE-model to the literature values (Ref. 26)

	Literature [Hz]	**FE-Model [Hz]**
1. Mode	7.66	7.66
2. Mode	15.24	15.24
3. Mode	38.80	38.80
4. Mode	55.33	55.33

In order to obtain a direct comparison of different methods based on the structural model used here, three additional aeroelastic analyses were carried out in addition to the UPM-HTModal coupling. Firstly, a DUST-HTModal coupling was implemented based on the principle of the UPM-HTModal coupling, and secondly, the existing DUST-MBDyn coupling from the Politecnico di Milano was used. Additionally, a flutter analysis (SOL145) was performed with NASTRAN.

For the time-resolved transient approaches (i.e. UPM-HTModal, DUST-HTModal, and DUST-MBDyn), a time step of 0.001s is used in each case. To investigate flutter instability, an initial angle of attack of 0.05° is applied as a perturbation in the transient methods, as in (Ref. 15) and (Ref. 27). For flutter analysis in NASTRAN, the p-k method is used.

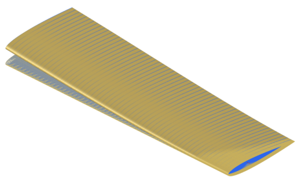

(a) 1. Flap (7.66 Hz)

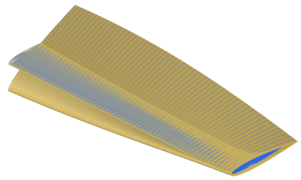

(b) 1. Torsion (15.24 Hz)

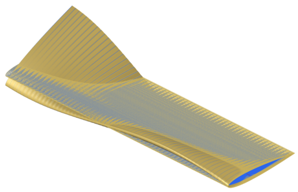

(c) 2. Torsion (38.80 Hz)

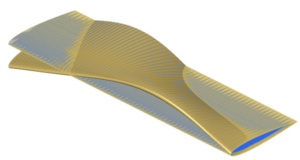

(d) 2. Flap (55.33 Hz)

Figure 7: First two flapping and torsional eigenmodes of the structural Goland wing model

Flutter Analysis

To determine the flutter speeds using the transient methods, a speed sweep was performed, and the corresponding time histories of the wing tip displacements were analysed with regard to damping in order to characterise stable or unstable behaviour. The flutter frequencies were also determined from the time histories. Figure 8 shows the z-displacements at the wing tip calculated with the UPM-HTModal coupling. The green line corresponds to a damped stable state below the flutter speed, while the red line shows unstable behaviour with bending-torsion instability and corresponds to a flow state above the flutter speed. The blue line shows the behaviour near the flutter speed with a free oscillation of constant amplitude. Figure 9 shows the deformation state that occurs in the case of bending-torsion flutter instability with the corresponding distributions of the pressure coefficient. These results demonstrate that the UPM-HTModal coupling is capable of correctly modelling fixed-wing flutter.

Table 3 compares the flutter speeds and frequencies determined using different methods and models. All aeroelastic couplings investigated in this work deliver similar results and also correspond well with comparable models from the literature, such as (Ref. 27). This shows that the UPM-HTModal coupling implemented here can predict fixed-wing flutter well and also correctly represents the three-dimensional aerodynamic effects that occur on wings with a low aspect ratio.

Table 3: Comparison of flutter speeds and frequencies for the Goland wing

Model	V_f $[ms^{-1}]$	f_f **[Hz]**
Analytical (Ref. 26)	137.2	11.25
SHARP,Beam+UVLM (Ref. 27)	165.0	10.98
DUST-MBDyn	162.3	10.95
DUST-HTModal	157.6	10.90
UPM-HTModal	155.1	11.70
NASTRAN SOL145	163.5	10.83

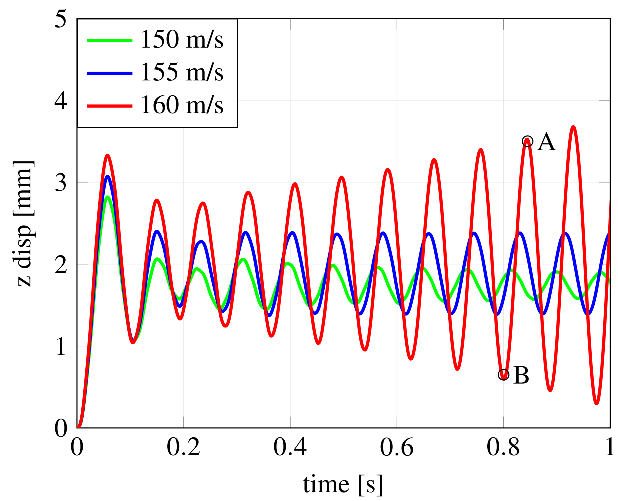

Figure 8: Comparison of the z-displacement at the tip of the Goland wing, simulated with the UPM-HTModal aeroelastic coupling framework at three different free stream velocities

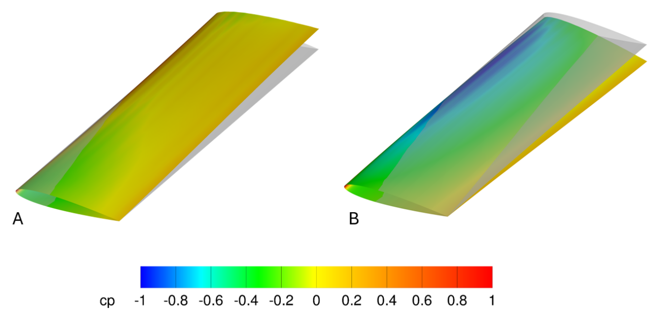

Figure 9: Deformed state of the Goland wing associated with the bending-torsion instability combined with the corresponding pressure coefficient distribution

PAZY WING

Setup and Models

The second test case investigated is the Pazy wing, which was specially designed at Technicon-IIT as an aeroelastic benchmark model for highly elastic structures with large deformations and which was thoroughly tested in a wind tunnel (Refs. 28,29). Flexible structures with comparatively large deformations are particularly relevant for new VTOL configurations and pose special challenges for aeroelastic prediction tools. In addition to the detailed test results, several simulation tools have already been tested and validated with the Pazy wing (Ref. 30). A simple design was chosen for the wing with a rectangular planform, without sweep and taper, and with a NACA0018 profile. The wing was clamped on one side for the wind tunnel tests and analysed at different flow velocities and angles of attack, with deformations of up to 50% of the span. In addition to static aeroelastic deformation tests, flutter tests were also carried out under various conditions. Figure 10 shows both the CAD model and the actual wing used for the test campaigns. The wing consists of a central aluminium plate and a 3D-printed chassis, which consists of evenly spaced ribs (NACA0018 shape), a leading and trailing edge stiffener bar, and a tip rod. For the outer aerodynamic shape, the wing was covered with Oralight polyester film. The primary load-bearing structure is the aluminium 7075 spar with a contribution of 85% to the total stiffness of the wing (Ref. 28). Table 4 summarises the basic properties of the Pazy wing and the test setup (Ref. 29).

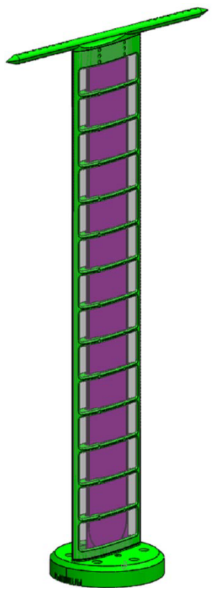

(a) CAD model

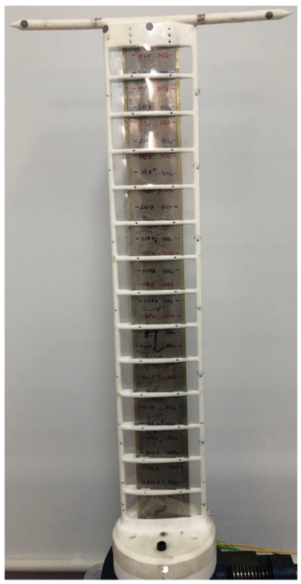

(b) Pazy wing

Figure 10: CAD model and real-life representation of the Pazy wing from (Ref. 28)

Table 4: Properties of the Pazy wing and flow condition (Ref. 28)

Wing properties	
Half span	550 *mm*
Chord (c)	100 *mm*
Tip rod length	300 *mm*
Tip rod diameter	10 *mm*
Airfoil	NACA0018
Main structure	Aluminium plate
	(550 x 60 x 2.25 mm)
Chassis structure	3D printed Nylon
Covering/Skin	Oralight
Overall mass	361 *g*
(with instrumentation)	
Flow condition	
Air density (ρ)	1.225 $kg\ m^{-3}$

For modelling the structure, a combination of beam and shell elements was chosen (see Fig. 11). The aluminium spar, the ribs of the chassis, and the outer skin are modelled using shell elements, while the chassis stiffeners at the leading and trailing edge and the tip rod are modelled using beam elements. The eigenfrequencies determined from the modal analysis of the FE-model are compared with the experimental values from the literature in Table 5 and show very good agreement in the undeformed state. The respective first four eigenmodes are shown in Figure 12. For the modelling of the aerodynamics, the wing was discretised with surface panels, using 30 panels in the spanwise direction and 40 panels in the chordwise direction with a half-cosine refined distribution at the leading edge.

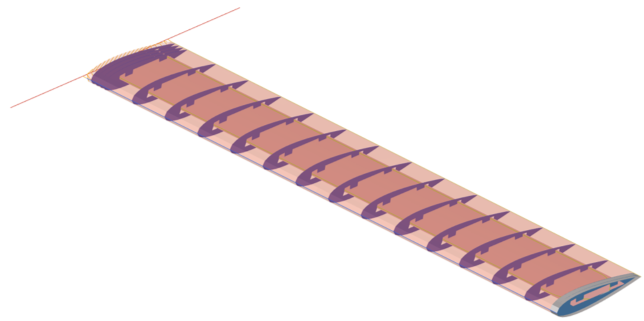

Figure 11: Representation of the structural Pazy wing model

Table 5: Comparison of the eigenfrequencies for the Pazy wing FE-model to the literature values (Ref. 28)

	Literature [Hz]	**FE-Model [Hz]**
1. Flap Bending	4.26	4.26
2. Flap Bending	28.5	28.51
1. Torsion	42.0	42.01
3. Flap Bending	81.5	81.52

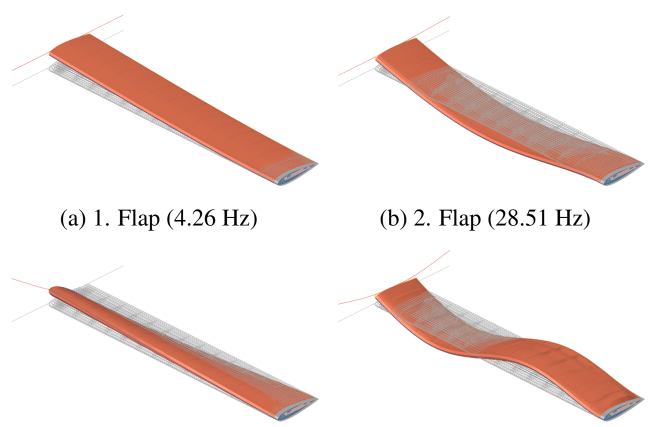

(a) 1. Flap (4.26 Hz)

(b) 2. Flap (28.51 Hz)

(c) 1. Torsion (42.01 Hz)

(d) 3. Flap (81.52 Hz)

Figure 12: First four eigenmodes of the structural Pazy wing model

A time step of 0.001s is used for the aeroelastic coupling, with a sub-cycling time step of 5e-4s for the aerodynamic solver UPM. In accordance with the damping values determined in the experiments (Ref. 28), a damping value of 0.2% was specified for the modal structural model.

Static Analysis

Prior to the dynamic flutter analysis, a static aeroelastic coupling was performed, in which the wing tip displacement in the z-direction was analysed for different free stream velocities and angles of attack and compared with the wind tunnel data. Two different velocities ($30m/s$ and $40m/s$) were investigated in the relevant AoA range. Figure 13 compares the curves for the different speeds and AoA. For both free stream velocities, the simulation results show very good agreement with the wind tunnel data, although it can be seen that, as expected, with increasing total deformation and the associated non-linearity, this is not adequately covered by the structural model.

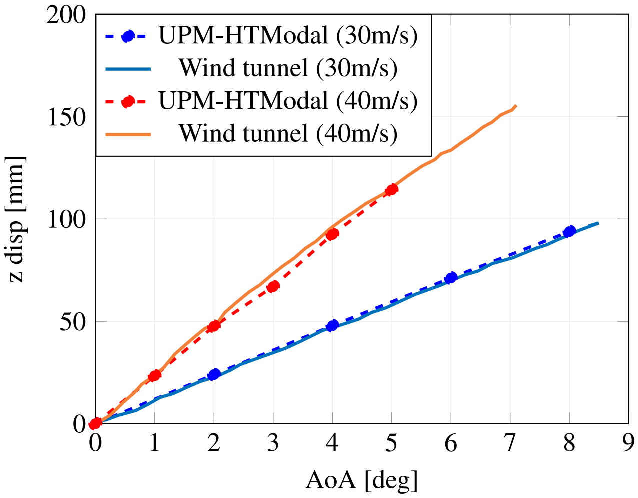

Figure 13: Comparison of the z-displacement at the tip of the Pazy wing between UPM-HTModal coupling simulation results and wind tunnel test data (Ref. 28) for two different free stream velocities ($30m/s$ and $40m/s$)

Flutter Analysis

To determine the flutter speeds using the UPM-HTModal coupling, a speed sweep was performed, and the corresponding time histories of the wing tip displacements were analysed with regard to damping in order to identify stable or unstable behaviour. An angle of attack of 3° was selected as the base configuration for the validation. The large deformations caused by the angle of attack and the flow velocities result in a significant change of the eigenfrequencies of the structure (see (Ref. 28)), which influences the aeroelastic behaviour around and above the flutter speed. However, since the specific area of application of the presented coupling framework is optimisation and design studies, in which the undeformed structure is usually used for modal analysis, it was decided here to investigate whether the flutter speed and stability behaviour can also be correctly predicted with the base modal model. Table 6 lists the flutter speed determined using the aeroelastic UPM-HTModal coupling in comparison to the experimentally determined flutter speed at a base AoA of 3°. The simulated result agrees very well with the experimentally determined flutter speed, which shows that the coupling framework can also correctly represent the stability behaviour of highly elastic components.

Table 6: Comparison of flutter speeds for the Pazy wing

Method	V_f $[ms^{-1}]$
Wind tunnel tests (Ref. 29)	49
UPM-HTModal	49.1

The investigations performed in this work have shown that the determined flutter speed of such highly elastic components depends heavily on the structural damping applied to the model, as also mentioned in (Ref. 31). This means that, especially for design studies for which the damping is usually not known, different damping coefficients have to always be investigated, and the sensitivity regarding the stability behaviour has to be carefully assessed and always considered. The wind tunnel tests carried out by Technicon additionally showed that the instability occurring between the second bending and first torsion mode represents a "hump mode". This means that the unstable mode becomes stable again at higher speeds. This behaviour could not be replicated by the coupling framework used, which is probably due to the use of the undeformed modal model. However, since the typical deformations in rotorcraft are usually below 20% of the span (this is the deformation occurring in the flutter range of the Pazy wing), it can be said that the approach used for UPM-HTModal is legitimate for rotorcraft applications and reliably predicts the possible instabilities that may occur in the relevant range, even for highly elastic components.

AREA BLADE

Setup and Models

For the final test case, a rotor is used to demonstrate the applicability of the coupling framework in rotating systems. The setup of the MERIT whirl tower test rig (see Fig. 14), which was developed by Heuschneider (Ref. 32) at the Institute for Rotorcraft and Vertical Flight, was chosen as a reference case. The test rig offers the possibility to investigate different blade geometries in a speed range of up to 3000rpm, with the option of performing measurements in both the non-rotating and rotating system through the use of an appropriate telemetry system. In addition, 3D deformation data of the investigated blades can be recorded using an optical measurement system and subsequent digital image correlation (DIC). For this purpose, reflective patches are affixed to the blades section by section across the radius, and their transient movement is then tracked using the *ARAMIS* photogrammetry system from *Carl Zeiss GOM Metrology GmbH*. However, previous tests have shown that the patches with a thickness of 0.3 mm have an influence on the aerodynamic performance of the blades, leading to a reduction in rotor thrust (Ref. 33).

The blade set used was the AREA blades developed at the institute, which were originally designed for the high-altitude

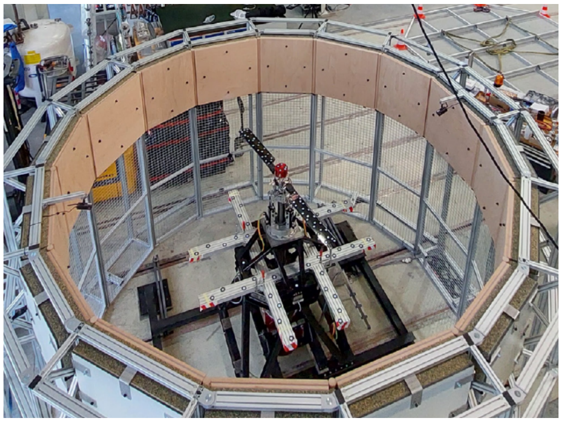

Figure 14: Whirl Tower test setup MERIT (Munich Experimental Rotor Investigation Testbed)

drone AREA of the same name, which was also developed at the Institute for Rotorcraft and Vertical Flight (Ref. 34). Figure 15 shows the general dimensions of the blade mounted on the whirl tower test rig. The blades are typically designed rotor blades with a C-spar design and a carbon fibre prepreg structure. A linear twist of -10° is applied across the entire radius with a pretwist at the hub of 7.5° to ensure that the same angle of attack applies at the 75% span position in the undeformed state as at the blade attachment. A NACA23012 profile with trailing edge tab was used for the airfoil shape. Due to the given radius of the blades and the limitation of the diameter of the housing, the flow and, in particular, the tip vortices are influenced by the housing. This influence increases with increasing pitch angle and leads to possible deviations in thrust and blade deformation. The effects and influencing factors are part of current research and investigations at the institute.

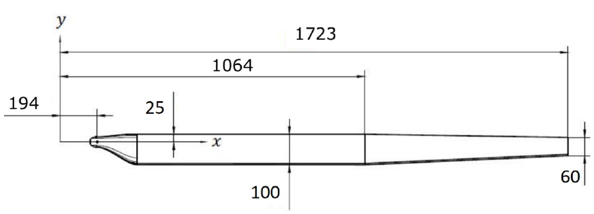

Figure 15: Geometrical planform data of the AREA blade

As with the Goland model, a combination of beam and shell elements was chosen for modelling the structure (see Fig. 16), in which the load-bearing structure is formed by the beam elements. These beam elements are connected to the shell elements, which exclusively represent the outer shape, via rigid body elements in the chord direction. For the transition between blade attachment and aerodynamic sections, a finer beam distribution was used than in the aerodynamic section part, to represent the stiffness characteristic and changes in that area adequately. The base data set regarding stiffness and mass distribution was determined using the blade design tool *SONATA* in combination with *ANBA* (Ref. 35) and then finally optimised and adjusted on the basis of experimental data (Ref. 34).

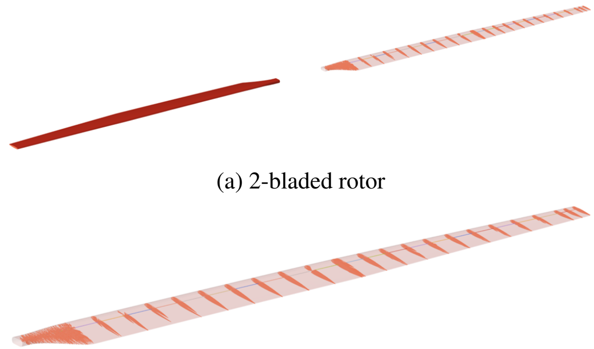

(a) 2-bladed rotor

(b) single blade

Figure 16: Representation of the structural AREA rotor and blade model

The eigenfrequencies determined in the stationary reference system from the modal analysis of the FE-model are listed in Table 7 and are compared with experimental data and *CAMRAD II* (CII) results. The experimentally determined frequencies were determined using a Laser-Doppler-Vibrometer (Ref. 34). The respective first six eigenmodes are shown in Figure 17. When comparing the determined eigenfrequencies between the FE-model and the experiment, a very good agreement can be seen.

Table 7: Comparison of the eigenfrequencies for the AREA FE-model to experiments and CAMRAD II results (Ref. 34) for the stationary reference system

	Tests [Hz]	**CII [Hz]**	**FE-Model [Hz]**
1. Flap	6.88	6.65	6.90
1. Lead-Lag	24.4	28.46	24.90
2. Flap	38.2	35.52	37.99
3. Flap	92.5	92.85	95.77
2. Lead-Lag	140.4	–	140.6
1. Torsion	147.6	–	147.7

For the use in the coupled rotor simulation, an additional FE modal analysis was performed in the rotating reference system, i.e. with a preloading corresponding to a load of $\Omega = 900 rpm$. The eigenfrequencies determined from this are listed in Table 8 and also compared with experimental data and CAMRAD II. For the experimental determination of the eigenfrequencies in the rotating reference system, an Operational Modal Analysis (OMA) was performed, combined with an Eigen System Realisation Algorithm (ERA) and based on the 3D blade deformation data from whirl tower tests (Ref. 36). This method was used to determine the first three flap eigenfrequencies. When comparing the determined eigenfrequencies, it can be seen that the FE modelling overestimates the first two flap modes, whereas the third mode is underestimated. The first eigenfrequency determined with CAMRAD II agrees much better with the experimentally determined data, while the remaining frequencies from CAMRAD II agree very well with the FE data.

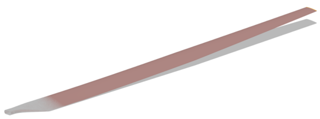

(a) 1. Flap (6.90)

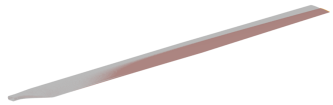

(b) 1. Lead-Lag (24.90 Hz)

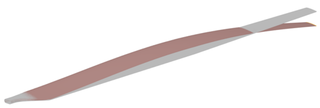

(c) 2. Flap (37.99 Hz)

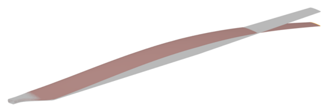

(d) 3. Flap (95.77 Hz)

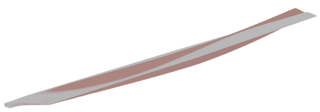

(e) 2. Lead-Lag (140.6 Hz)

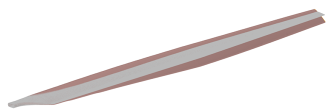

(f) 1. Torsion (147.7 Hz)

Figure 17: First six eigenmodes of the structural AREA blade model in the stationary reference system

For aerodynamic modelling, the blades were discretised using surface panels, with 15 panels in the radial direction and 30 panels in the chord direction with a half-cosine refined distribution at the leading edge. A step size of 2° azimuth angle was selected for the aeroelastic coupling, which corresponds to a time step of ~ 0.0004s.

Table 8: Comparison of the eigenfrequencies for the AREA FE-model to whril tower tests (Ref. 36) and CAMRAD II results (Ref. 34) for the rotating reference system (900rpm)

	Test [Hz]	CII [Hz]	FE-Model [Hz]
1. Flap	17	17.45	18.36
1. Lead-Lag	–	29.90	30.32
2. Flap	49	53.80	54.04
3. Flap	117	113.4	113.1

Static Analysis

The test case examined is a hover test at a rotational speed of $\Omega = 900 rpm$, which corresponds to a blade tip speed of $v_{tip} = 162 m/s$. The aeroelastic behaviour of the AREA blades was examined at different collective pitch angles in a range between 2° and 8°. For the comparison between whirl tower tests and the simulated results of the coupling, the bending line of the c/4 line (z-displacement of the individual radial positions) was used over the radius. The results are plotted in Figure 18. There is good agreement between the coupling data and the experimental data, with an overall maximum deviation at the blade tip of 6% at a collective angle of 8°. With increasing collective angle, the coupling simulation slightly overestimates the blade deformation. This is due to the fact that the simulation has a tendency to overestimate the generated thrust more and more as the collective angle increases. The reason for this is probably the increasing influence of interactions with the housing and the influence of the patches. Overall, however, both the qualitative course of the bending line and the absolute displacements are well represented by the simulation, which demonstrates the applicability of the UPM-HTModal framework to rotating components.

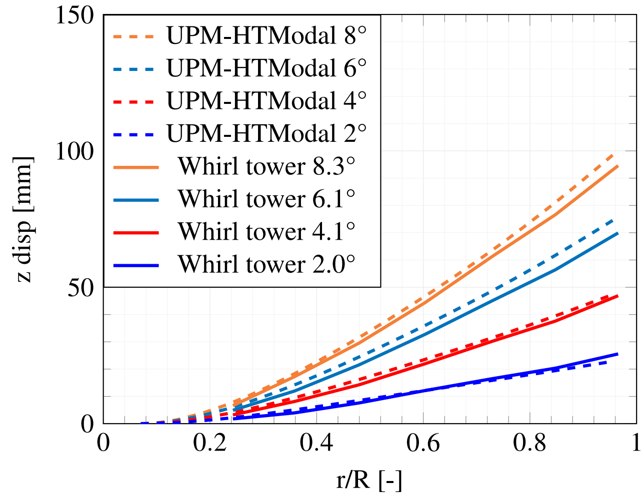

Figure 18: Comparison of the z-displacement along the rotor radius of the AREA rotor between UPM-HTModal coupling simulation results and MERIT whirl tower data (Ref. 33) for different collective blade pitch angles

CONCLUSIONS

This study presents a mid-fidelity aeroelastic coupling framework based on a surface-based coupling between the aerodynamic solver UPM and the modal structural solver HTModal. The framework is validated using various benchmark and experimental cases, including the Goland and Pazy wings and hover tests with AREA rotor blades on the MERIT whirl tower test rig at the Institute for Rotorcraft and Vertical Flight.

The results show that the coupling approach is capable of reliably predicting static deformations for both wing structures and rotating components. Furthermore, it can be demonstrated that dynamic stability characteristics and the occurrence of flutter for wing structures can also be predicted correctly. For the Goland and Pazy wings, the calculated flutter speeds and frequencies show very good agreement with analytical, numerical, and experimental reference data. In the rotor application, the simulated blade deformations at different collective pitch angles can be reproduced with deviations of less than 6% from the measurements, confirming the suitability of the framework for rotating systems as well. Due to the lack of available data, no stability investigations could be carried out in the rotating system.

The results underscore the potential of the presented framework as an efficient and versatile tool for aeroelastic analyses in rotorcraft applications. For future developments, further investigations are to be carried out in the rotating system, for example with cyclic inputs, in order to validate the framework beyond stationary hover conditions. In addition, simulations of more complex setups, such as rotor-wing configurations or entire helicopter and VTOL simulations, will be carried out in order to apply and test the method in highly interactive flow conditions. Furthermore, the aforementioned tool chain with SONATA, ANBA, and the aeroelastic coupling will be further optimised and automated in order to obtain a comprehensive tool for the design of rotor and propeller blades and to improve the prediction accuracy.

Author contact:
Moritz Linder moritz.linder@tum.de

REFERENCES

1. Wachspress, D. A., Quackenbush, T. R., and Boschitsch, A. H., “Rotorcraft interactional aerodynamics with fast vortex/fast panel methods,” *Journal of the American Helicopter Society*, Vol. 48, No. 4, 2003, pp. 223–235.

2. Barkai, S. M., Rand, O., Peyran, R. J., and Carlson, R. M., “Modeling and analysis of tilt-rotor aeromechanical phenomena,” *Mathematical and Computer Modelling*, Vol. 27, No. 12, 1998, pp. 17–43.

3. Lorber, P. F., Min, B.-Y., and Wake, B. E., “Interactional aerodynamic insight obtained from wind tunnel testing and computational analysis,” 74th Annual Forum of the American Helicopter Society, Phoenix, AZ, 2018.

4. Whitehouse, G. R., Boschitsch, A. H., and Keller, J. D., “Development and testing of a lagrangianeulerian cfd analysis for moving body and interactional aerodynamics analysis,” *AIAA Scitech 2019 Forum*, 2019, pp. 2117.

5. Prouty, R., “The yah-64 empennage and tail rotor-a technical history,” American Helicopter Society 38th Annual Forum, St. Louis, Missouri, 1982.

6. K. C. Hansen, “Handling Qualities Design and Development of the CH-53E, UH-60A, and S-76,” Royal Aeronautical Society International Conference on Helicopter Handling Qualities and Control, London, UK, November 1988.

7. Mazzucchelli, C. and Wilson, F., “The Achievement of Aerodynamic Goals on the EH101 Project through the Single Site Concept,” Proceedings of the 17th European Rotorcraft Forum, Berlin, Germany, September 1991.

8. Cao, Y. H., Wu, Z. L., and S., H. J., “Numerical Simulation of Aerodynamic Interactions among Helicopter Rotor, Fuselage, Engine and Body of Revolution,” *Science China Technological Sciences*, Vol. 57, No. 6, 2014, pp. 1206–1218.

9. O’Brien, D. and Smith, M., “Analysis of Rotor-Fuselage Interactions Using Various Rotor Models,” Proceedings of the 43rd Aerospace Sciences Meeting, Reno, NV, January 2005.

10. Renaud, T., O’Brien, D., Smith, M., and Potsdam, M., “Evaluation of Isolated Fuselage and Rotor-Fuselage Interaction Using CFD,” American Helicopter Society 60th Annual Forum Proceedings, Baltimore, MD, June 2004.

11. Guo, T., Lu, D., Lu, Z., Zhou, D., Lyu, B., and Wu, J., “CFD/CSD-based flutter prediction method for experimental models in a transonic wind tunnel with porous wall,” *Chinese Journal of Aeronautics*, Vol. 33, No. 12, 2020, pp. 3100–3111.

12. Schäferlein, U., Keßler, M., and Krämer, E., “Aeroelastic Simulation of the Tail Shake Phenomenon,” *Journal of the American Helicopter Society*, Vol. 63, No. 3, 2018, pp. 1–17.

13. Rinker, M., Ries, T., Embacher, M., Platzer, S., Uhl, G., and Hajek, M., “Simulation of Rotor–Empennage Interactional Aerodynamics in Comparison to Experimental Data,” Vertical Flight Society 75th Annual Forum & Technology Display, Philadelphia, Pennsylvania, May 2019.

14. Alvarez, E. J. and Ning, A., “Development of a Vortex Particle Code for the Modeling of Wake Interaction in Distributed Propulsion,” AIAA Applied Aerodynamics Conference, Atlanta, GA, USA, June 2018.

15. Savino, A., Cocco, A., Zanotti, A., Tugnoli, M., Masarati, P., and Muscarello, V., “Coupling Mid-Fidelity Aerodynamics and Multibody Dynamics for the Aeroelastic Analysis of Rotary-Wing Vehicles,” *Energies*, Vol. 6979, No. 14, 2021.

16. Linder, M., Yurt, M. K., and Yavrucuk, I., “Development of a Mid-Fidelity Aeroelastic Coupling Framework for Analyzing Rotor-Airframe Interactions,” 49th European Rotorcraft Forum, Bueckeburg, Germany, September 2023.

17. Kunze, P., “Evaluation of an Unsteady Panel Method for the Prediction of Rotor-Rotor and Rotor-Body Interactions in Preliminary Design,” 41st European Rotorcraft Forum, Munich, Germany, September 2015.

18. J. P. Yin and S. R. Ahmed, “Helicopter Main-Rotor/Tail-Rotor Interaction,” *Journal of the American Helicopter Society*, Vol. 45, No. 4, 2000, pp. 293–302.

19. S. R. Ahmed and V. T. Vidjaja, “Unsteady Panel Method Calculation of Pressure Distribution on BO 105 Model Rotor Blades,” American Helicopter Society’s 50th Annual Forum, Washington, DC, May 1994.

20. Yin, J. and Kunze, P., “DLR Free Wake Unsteady Panel Method (UPM): User Guide,” .

21. Kunze, P., “Approximate Boundary Layer Methods for a 3D Panel Code for Helicopter Simulations,” 19th ONERA-DLR Aerospace Symposium, Meudon, France, June 2019.

22. Tugnoli, M., Montagnani, D., Syal, M., Droandi, G., and Zanotti, A., "Mid-fidelity approach to aerodynamic simulations of unconventional VTOL aircraft configurations," *Aerospace Science and Technology*, Vol. 115, 2021, pp. 106804.

23. Humar, J., *Dynamics of Structures, Third Edition*, CRC Press, Hoboken, 3rd ed., 2012.

24. Schäferlein, U., *Numerical Investigation of Aeroacoustic and Aeroelastic Phenomena on a Helicopter Using Higher-Order Methods*, Verlag Dr. Hut, 1st ed., 2018.

25. Chourdakis, G., Davis, K., Rodenberg, B., Schulte, M., Simonis, F., Uekermann, B., Abrams, G., Bungartz, H., Cheung Yau, L., Desai, I., Eder, K., Hertrich, R., Lindner, F., Rusch, A., Sashko, D., Schneider, D., Totounferoush, A., Volland, D., Vollmer, P., and Koseomur, O., "preCICE v2: A sustainable and user-friendly coupling library [version 2; peer review: 2 approved]," *Open Research Europe*, Vol. 2, No. 51, 2022.

26. Goland, M., "The flutter of a uniform cantilever wing," *Journal of Applied Mechanics*, Vol. 12, No. 4, 1945, pp. 197–208.

27. Murua, J., Palacios, R., and Graham, J. M. R., "Assessment of Wake-Tail Interference Effects on the Dynamics of Flexible Aircraft," *AIAA Journal*, Vol. 50, No. 7, 2012, pp. 1575–1585.

28. Avin, O., Raveh, D. E., Drachinsky, A., Ben-Shmuel, Y., and Tur, M., "Experimental Aeroelastic Benchmark of a Very Flexible Wing," *AIAA Journal*, Vol. 60, No. 3, 2022.

29. Drachinsky, A., Avin, O., Raveh, D. E., Ben-Shmuel, Y., and Tur, M., "Flutter Tests of the Pazy Wing," *AIAA Journal*, Vol. 60, No. 9, 2022.

30. Ritter, M., Hilger, J., Ribeiro, A., Öngüt, A. E., Righi, M., Raveh, D. E., dos Santos, L. G. P., Drachinsky, A., Riso, C., Cesnik, C. E., Stanford, B., Chwalowski, P., Kovvali, R. K., Duessler, S., Cheng, K. C., Palacios, R., dos Santos, J. P., Marques, F. D., Begnini, G. R. R., Verri, A. A., Lima, J. J., de Melo, F. B., and Bussamra, F. L., *Collaborative Pazy Wing Analyses for the Third Aeroelastic Prediction Workshop*.

31. Drachinsky, A. and Raveh, D. E., "Nonlinear Aeroelastic Analysis of Highly Flexible Wings Using the Modal Rotation Method," *AIAA Journal*, Vol. 60, No. 5, 2022, pp. 3122–3134.

32. Heuschneider, V., *Structural Loads of a Mach-Scaled Rotor in Dynamic Stall – An Experimental Hover Analysis*, Ph.D. thesis, Technical University Munich, 06 2024.

33. Mitropoulos, M., Heuschneider, V., Barth, A., and Yavrucuk, I., "Experimental Whirl Tower Tests Approaching and Surpassing Stall for a Variety of Tip Speeds and Rotor Blades," 05 2024.

34. Barth, A., *Auslegung, Simulation, Bau und Flugerprobung eines unbemannten, elektrischen Hubschraubers mit kämmenden Rotoren für extreme Flughöhen*, Ph.D. thesis, Technical University Munich, 05 2020.

35. Feil, R., Pflumm, T., Bortolotti, P., and Morandini, M., "A cross-sectional aeroelastic analysis and structural optimization tool for slender composite structures," *Composite Structures*, Vol. 253, 2020, pp. 112755.

36. Aslandogan, O. H., Mitropoulos, M., and Yavrucuk, I., "Operational Modal Analysis using modified Eigensystem Realization Algorithm on Whirl Tower Data," 51st European Rotorcraft Forum, Venice, Italy, September 2025.